ACCEPT/REJECT CRITERIA FOR STRUCTURAL CERAMICS:

PART 3: PROBABILISTIC MODELS FOR INCLUSION INITIATED FRACTURE IN CERAMICS

A.G. Evans
University of California
Berkeley, California 94720

B.I. Davis and G. Meyer
Rockwell International Science Center
Thousand Oaks, California 91360

H.R. Baumgartner
Norton Co.
Worcester, Massachusetts

ABSTRACT

Fracture tests on hot-pressed silicon nitride containing several types of inclusions have been conducted. Fracture models pertinent to each inclusion type have been proposed and correlated with the data. The resultant fracture probability relations are one of the key inputs to accept/reject decisions for nondestructive failure prediction.

INTRODUCTION

Inclusions can be an important source of failure in structural ceramics. It is crucial for the structural utilization of these materials that the probability of fracture from typical inclusions be sufficiently characterized that effective nondestructive failure prediction schemes be devised. In this study, samples of silicon nitride containing typical inclusions are subjected to controlled fracture tests to determine both the fracture mechanism and the specific fracture stress at the inclusion. Fracture models pertinent to each inclusion type are then developed, and the fracture probability (derived from the test data) is related to the parameters of the model. The resultant probability functions constitute one of the three functions required to isolate the accept/reject criterion pertinent to nondestructive failure prediction.[1]

Preliminary studies of fracture from inclusions in ceramics[2,3] have indicated that the fracture process is likely to consist of the activation of small defects (voids, disbonds, grain boundary cracks), occurring within or near the inclusion, by the ambient local stress field associated with the thermal expansion mismatch and the applied stress. Usually, the influence of the inclusion on strength is expected to be less severe than that of a crack of equivalent dimensions.[2] The important exception is an inclusion with both a thermal expansion coefficient and a shear modulus lower than the host material (then, large radial cracks can develop that substantially reduce the strength). However, the incidence of such inclusions in structural ceramics such as silicon nitride is expected to be minimal, because these materials have a low intrinsic thermal expansion coefficient.

The inherent flaws that initiate inclusion fracture are likely to be statistically distributed in size and space. Therefore, the fracture stress should not be expected to relate uniquely to the inclusion dimensions; but rather, to exhibit a distribution of values for each inclusion size, as found for fracture from voids.[4,5] The determination of the fracture distribution functions is the primary objective of the present study.

EXPERIMENTAL

Technique

Samples containing the inclusion types that predominate in hot-pressed silicon nitride (Table I) were specially fabricated* in the form of 2.54 cm diameter discs, with the inclusions approximately located in the disc center. The samples were inspected using advanced ultrasonic techniques[6,7] to determine the precise location of the dominant inclusion. The samples were then machines until the defect was located ~ 200μm from one surface of the sample. This operation was conducted to ensure that the defect would be subjected to an appreciable tensile stress during subsequent flexure testing. Thereafter, each sample was annealed, in air at 1000°C for ~ 20 hr., to minimize the influence of surface cracks introduced during the grinding process. Finally, the samples were subjected to flexural, constant displacement-rate fracture tests, conducted at room temperature. Those samples with defects located at the disc center were tested in biaxial flexure.[8] Samples with defects displaced from the disc center were cut into beams (20 cm x 5 mm x 5 mm), such that the defect was located at the beam center, and then tested in three-point flexure. Acoustic emission was monitored on each sample throughout the test.

*The fabrication was conducted by the Norton Co., Worcester, Massachusetts.

TABLE I

Inclusion Type	Stress at Inclusion (MPa)	Inclusion Size z(μm)	x(μm)	V(m^3)
Silicon	401	50	265	-
	362	100	475	-
	375	75	425	-
	264	125	625	-
	243	250	875	-
	283	125	875	-
	272	250	675	-
	410	75	200	-
	432	75	275	-
	284	175	425	-
	357	100	100	-
	424	75	250	-
	434	50	100	-
	265	175	750	-
	252	125	625	-
Iron	398			2.5×10^{-12}
	323			1.6×10^{-11}
	383			9.1×10^{-12}
	334			2.2×10^{-11}
	355			3.1×10^{-11}
	210			6.2×10^{-13}
	217			7.0×10^{-11}
	404			6.2×10^{-13}
	258			7.0×10^{-11}
	296			6.1×10^{-11}
	333			3.3×10^{-4}
	283			6.5×10^{-11}
	173			2.9×10^{-10}
	281			1.1×10^{-19}
	206			3.2×10^{-10}
	190			1.8×10^{-10}
Tungsten Carbide	550	75	175	
	590	125	150	
	560	75	300	
	610	400	675	
	600	100	300	
	480	400	400	

Results

The results of the fracture tests were used to calculate the stress at the center plane of the defect, at the condition of fracture instability. These defect fracture stresses are summarized in Table I. The acoustic emission record did not generally indicate well-defined pre-fracture emission; except for the silicon inclusions, which exhibited consistent emission at about one-tenth of the final fracture load.

The dimensions of the fracture initiating defects on the fracture plane were measured on each sample, as summarized in Table I. Also, for samples in which defect removal could be effected, the defect volumes were measured. The detailed volume measurement technique is described in Appendix II. The results are summarized in Table I.

FRACTURE MODELS

General Considerations

It is instructive to provide a perspective of inclusion fracture by examining the stress fields associated with inclusions; and thereby, to identify the possible modes of fracture. (The fracture modes that occur for inclusions with a lower expansion coefficient than the matrix are excluded from consideration, as noted in the Introduction.)

The thermal expansion mismatch introduces hydrostatic tension within the inclusion. The magnitude of this stress, σ_α, is given by[9]

$$\sigma_\alpha = \frac{4G_M \Delta\alpha_\Delta T}{1 + [2(1-2\nu_i)/(1+\nu_i)](G_m/G_i)} \equiv \beta^* \quad (1)$$

where Δ_α is the differential in thermal expansion coefficients, ΔT is the temperature differential, G is the shear modulus, ν is Poisson's ratio and the subscripts m and i refer to the matrix and inclusion, respectively. The equivalent stresses within the matrix are, for a spherical inclusion:

$$\sigma_{rr} = \beta^* (a/r)^3 \qquad (2)$$

$$\sigma_{\theta\theta} = \beta^* (a/r^3)/2$$

The application of a stress σ_∞ also generates stresses in the inclusion. For a spherical inclusion and an applied pressure P_∞, the stress in the inclusion is given by[10]:

$$\frac{P_i}{P_\infty} = 1 + \left(\frac{2}{3}\right)\frac{[(K_i/K)-1](1-2\nu)}{(1-\nu)}\left[\frac{4G+3}{4G+3K_i}\right] \equiv \psi \quad (3)$$

where K is the bulk modulus.

The significance of these local stresses depends on the distribution of flaws within the inclusion, matrix and interface; as well as the intrinsic toughness of the inclusion and the matrix. When the toughness of the inclusion is appreciably larger than that of the matrix (as might pertain for WC inclusions in Si_3N_4), fracture will tend to initiate within the matrix, from flaws located either at the interface or within the matrix itself (Fig. 1). In this case, the location of fracture and the fracture probability depend primarily on the ratio of the inclusion and matrix elastic constants. Specifically, for inclusions with a smaller modulus than the matrix, the maximum local tensile stress occurs at the equatorial plane,[11] and fracture will initiate from flaws located in this vicinity, as indicated in Fig. 1(a). For inclusions with a higher modulus than the matrix, the maximum local tension (in the appropriate orientation for continued extension into the matrix, i.e., normal to σ_∞) occurs at the poles of the inclusion[11] (Fig. 1(b)). However, both the maximum tension and the extent of the tensile zone are appreciably smaller (for the same modulus mismatch) than the equivalent quantities for the low modulus inclusions. The

probability of fracture from the latter is thus anticipated to be relatively low.

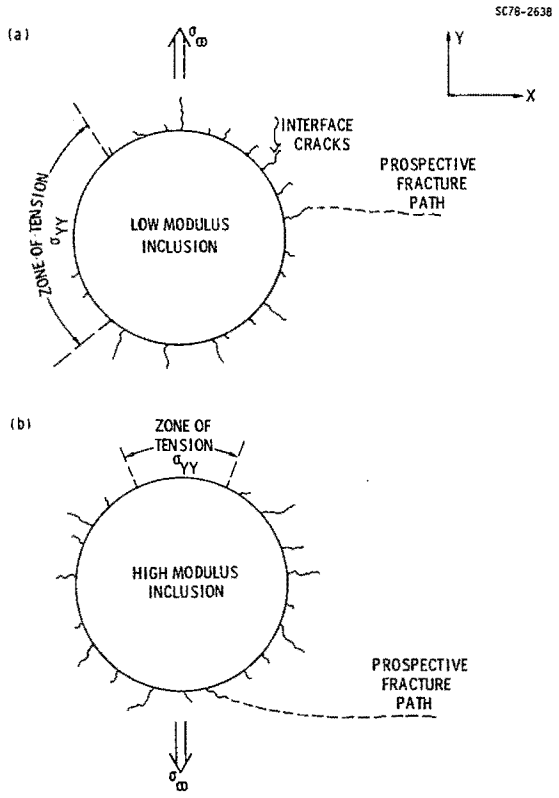

Fig. 1 Schematics indicating fracture initiated within the matrix from interface microcracks for (a) low modulus inclusions and (b) high modulus inclusions.

A more typical condition involves inclusions with a lower fracture toughness than the matrix. Then, inclusion fracture is likely. When the inclusion has a relatively high modulus (although not necessarily higher than that of the matrix), so that appreciable stresses develop within the inclusion, the fracture of the inclusion can be subcritical, i.e., an additional stress is required to initiate structural failure. Alternatively, if the inclusion has a low modulus (e.g., a porous inclusion, see Appendix I), the stress within the inclusion is low and inclusion fracture might then coincide with structural failure.

This multiplicity of fracture modes requires that each inclusion type be evaluated on an individual basis. The subsequent analysis comprises separate sections for each of the inclusion types listed in Table I.

Specific Fracture Models

Silicon Inclusions. The silicon inclusions are characterized by a lack of porosity, signifying that there is little thermal expansion mismatch at temperatures above ~1000°C (the temperature at which stress relaxation by mass transport becomes slow). This can be rationalized by noting that the large thermal contraction of the silicon between 1000 and 1800°C is counteracted by the unusual volume expansion that occurs during solidification. Between 1000° and 30°C the total contraction of the silicon is very similar to that of silicon nitride: indicating that the thermal mismatch stresses in the silicon inclusions should be small.

Dense silicon has elastic properties appreciably lower than those of silicon nitride (Youngs moduli of 110 and 320 GPa, respectively). These relative properties lead to a stress in the inclusion $\sigma_i \approx 0.64\ \sigma_\infty$ (see Eqn. 3). However, silicon has a very low fracture toughness (0.6 MPa$\sqrt{m}$) compared with the silicon nitride matrix (5 MPa$\sqrt{m}$); so that, despite the low stress level in the inclusion, the inclusion is liable to fracture before the matrix. This interpretation is consistent with the acoustic emission measurements (Section 2).

The subcritical fracture of the silicon inclusion introduces a crack with dimensions dictated by the dimensions of the inclusion. The cracked inclusion produces a complex stress intensification of the type[11]:

$$K_I = Z(a/c)F(G_i/G)\sigma_\infty a^\beta \qquad (4)$$

where Z is a function of the crack shape, F is a function of the relative elastic moduli and β is a constant ranging from 0.3 to 0.7. The present fracture model is developed on the premise that the modulus mismatch is small and that the crack inclusion can be treated as a crack in a homogeneous body. (This simplification is necessary at the present level of comprehension of the crack/inclusion problem, and will evidently introduce an error into the fracture characterization.) Then, introducing the macro-toughness of silicon nitride and the inclusion dimensions (on the fracture surface), a predicted fracture stress σ_p can be obtained from Eqn. (4).

$$\sigma_p = \frac{K_c}{Z(a/c)\sqrt{a}} \qquad (5)$$

The predicted stress for each sample is plotted in Fig. 2 as a function of the measured fracture stress. A reasonable correlation is apparent.

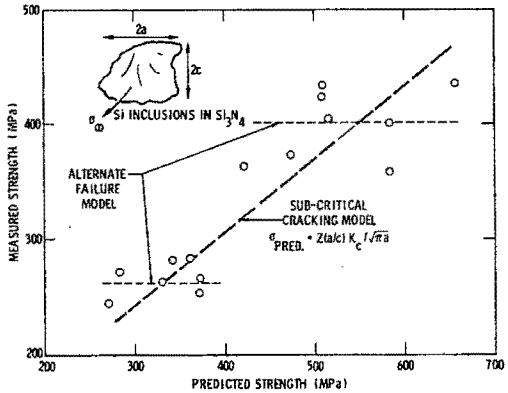

Fig. 2 A plot of the measured fracture strength of silicon nitride containing silicon inclusions as a function of the strength predicted by the subcritical cracking model.

A detailed statistical analysis has also been conducted to determine the level of correlation between the test data and the model. For this purpose, it has been supposed that the primary source of the variability in the measured strength is the variation in fracture toughness of the matrix circumventing the inclusion (which could be very difference from that of the remote matrix, because of an interaction zone). The inclusion/crack size is appreciably larger than the grain size; hence, the variability in toughness might be anticipated to conform to a normal distribution. The fracture data are thus analyzed to determine their conformance to the normal distribution.

The hypothetical model can be formally expressed as:

$$P_r[S \le \zeta | \sigma_p = x] = \frac{1}{v\sqrt{2\pi}} \int_{-\infty}^{\zeta} \exp\left[-\frac{1}{2}\left(\frac{y-(\alpha+\beta x)}{v}\right)^2\right] dy \qquad (6)$$

where v^2 is the variance of the strength S for any given σ_p and P_r is the conditional distribution of strengths S; note that the conditional expectation of S, given σ_p, is assumed to be a linear function of σ_p,

$$(S|\sigma_p = X) = \alpha + \beta X + \varepsilon \qquad (7)$$

where ε is a random variable having mean zero and variance v^2. Applying the usual null hypothesis tests to the available data is complicated by the fact that the fracture data comprise 15 observations of 12 random variables. Specifically, only the residual

$$e = (S|\sigma_p = x) - \hat{\alpha} - \hat{\beta} x \qquad (8)$$

can be observed, where $\hat{\alpha}$ and $\hat{\beta}$ are the maximum likelihood estimates of α and β. (An alternative hypothesis attributes the strength variability to variations in the shape of the crack at the criticality; this possibility is not examined in the present analysis.

The normality of the fracture data are thus analyzed using two approaches: (a) by disregarding the variance-convariance structure of the residuals and (b) by obtaining independent residual observations using an orthogonal transformation of the fracture data.

The first method of analysis assumes that these residuals are independent. The variation in the magnitude of the residuals with the magnitude of the observation can then be obtained directly, as plotted in Fig. 3. There does not appear to be a systematic trend in the residuals (as verified by values of α_1 (skewness) = 0.04 and α_2 (excess) = -0.93), indicating that the normality hypothesis may be reasonable. Also, if the residuals arranged in increasing order of magnitude are plotted (Fig. 5) against the expected value of the i'th order statistic, for a random variable having a standard normal distribution, the good linearity of the plot tends to support the contention that the residuals are observations of a random variable having a normal distribution. Separate analysis of the data at large and small σ_p, using a procedure proposed by Goldfeld and Quandt[12], indicates that the residuals exhibit a systematic increase with increasing magnitude of the observation. This does not invalidate the normality of the distribution, but suggests a variance that increases as σ_p increases; a result that can be tentatively rationalized, as discussed below. However, it should be noted that the data can also be shown to conform with similar confidence to a model in which the measured strength is independent of σ_p, but at two separate levels; one at $S \approx 263$ MPa for $\sigma_p < 400$ MPa, and the other at $S \approx 413$ MPa for $\sigma_p > 400$ MPa (Fig. 3). The data analysis does not, therefore, provide a unique confirmation of the proposed fracture model.

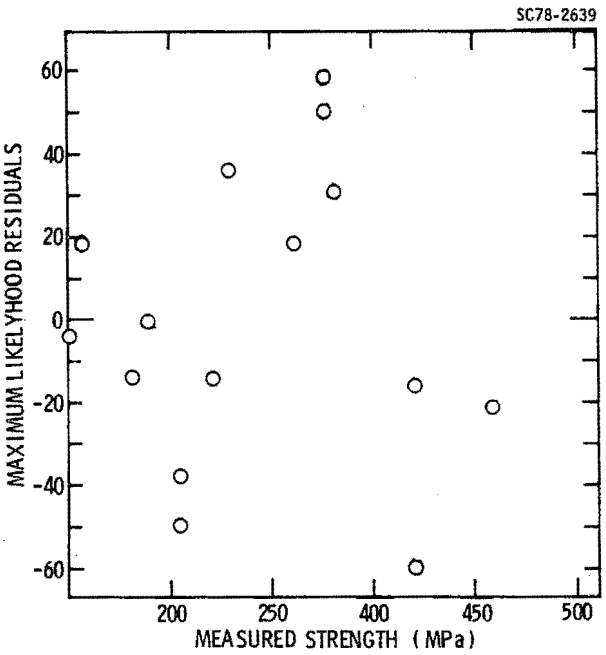

Fig. 3 A plot of the maximum likelihood residuals as a factor of the measured strength.

The second method of analysis uses a procedure proposed by Henry Theil.[13] It involves an orthogonal transformation through an identity matrix. Only 13 residuals can be obtained because 2 degrees of freedom (slope and intercept) are sacrificed in the estimation procedure. The residuals obtained in this fashion exhibit precisely the same trends as the maximum likelihood residuals, as exemplified in Fig. 4.

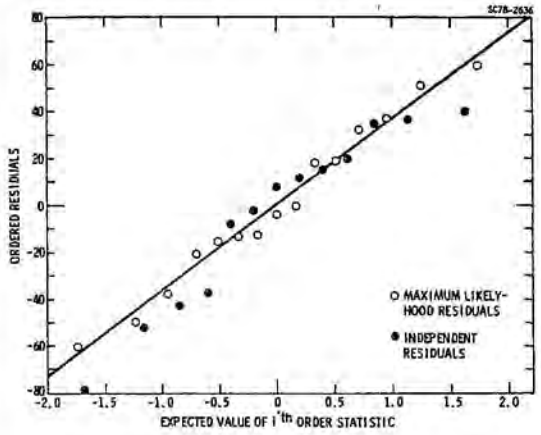

Fig. 4 A plot of the ordered residuals as a function of the estimate of the order statistics for both the maximum likelihood and the independent residuals.

It may be concluded, therefore, that the hypothesized fracture model, modified to allow for an increasing variance with increase in strength level, cannot be rejected by the data. However, this does not discount the possibility that the data might also be consistent with an alternate fracture model. If the assumed fracture model is indeed valid, the parameters of the model implied by the data are: α = 99.655 MPa, β = 0.541. The deviation of β from unity suggests, within the context of the model, that the local toughness of the matrix may be lower than the remote macro-toughness of the matrix (i.e., ~ 3 MPa$\sqrt{m}$ instead of 5 MPa$\sqrt{m}$). This effect can be justified on the basis of a matrix locally degraded by interaction with the inclusion. The relative extent of the degradation may also be supposed to increase as the inclusion size decreases, to account for the observed increase in variance with increase in the level of strength.

Iron Inclusion

Examination of the iron inclusions (Fig. 5) indicates that the inclusions contain several open cracks and/or porosity.

Fig. 5 A scanning electron micrograph of a fractured iron inclusion in hot-pressed silicon nitride.

The cracks and pores are presumably formed by diffusion within the inclusion (while at the elevated temperatures) to relieve the stresses introduced by thermal expansion mismatch (Appendix I). An unrelieved thermal expansion mismatch strain ε_α will, of course, still develop at temperatures below those capable of sustaining rapid mass transport. The presence of the open cracks reduces the effective bulk modulus of the inclusion. The stress within the inclusions, induced by the applied stress (Eqn. 3) and the thermal expansion mismath, should thus be appreciably lower than would be anticipated from the intrinsic modulus of the iron silicide material that comprises the inclusion. The proposed fracture model for these inclusions thus supposes that a critical fracture condition is attained when the stress within the inclusion reaches the level required to extend one of the internal cracks, i.e., that there is no subcritical inclusion fracture event. This hypothesis would be consistent with the lack of detectable acoustic emission prior to final fracture. The stress within the inclusion is a relatively uniform, hydrostatic tension p_i (or exactly uniform for an ellipsoidal inclusion) given by:

$$p_i = \psi \sigma_\infty + G_i^e \varepsilon_\alpha \tag{9}$$

where G_i^e is the effective shear modulus of the inclusion. A weakest link model of inclusion fracture for a state of uniform tension would indicate a fracture probability,[14]

$$\Phi_i = 1 = \exp\left[-V_i \int_0^{P_i} g(S)dS\right] \tag{10}$$

where V_i is the volume of the inclusion and $g(S)dS$ is the distribution of flaw strengths that relates to the distribution of cracks within the inclusion (and the toughness of the inclusion). If we adopt the Weibull assumption, that $g(S)$ is given by:

$$\int_0^{P_i} g(S)dS = \left(\frac{P_i^c}{P_o}\right)^k \tag{11}$$

where p_o is a scale parameter and k a shape parameter, the inclusion fracture probability becomes:

$$\Phi_i = 1 - \exp\left[-V_i \left(\frac{\psi\sigma_\infty^c + G_i^e}{P_o}\right)\right]^k \tag{12}$$

where σ_∞^c is the applied stress at fracture. The available data are not well suited for comparison with the predictions of this model, because each datum is obtained for a different V_i. Hence, a fracture probability cannot be uniquely assigned to each strength result. However, as a very approximate assessment of the utility of this model, a fracture probability is obtained by assuming it to be given by the order statistic based on the level

of the measured strength, regardless of the inclusion volume. The results are plotted in Fig. 6, as $-\ln(1-\Phi_i)$ vs. σ_∞^C. The curvature is presumed to signify an appreciable contribution from ε_α. The magnitude of $\varepsilon_\alpha G_i^e$ is estimated to be, $100/\psi$ MPa (Fig. 6), and the corresponding value of k is ~ 11. Both values are reasonable. Additional experiments in which V_i is essentially invariant must be conducted, however, if a rigorous evaluation of the model is to be effected.

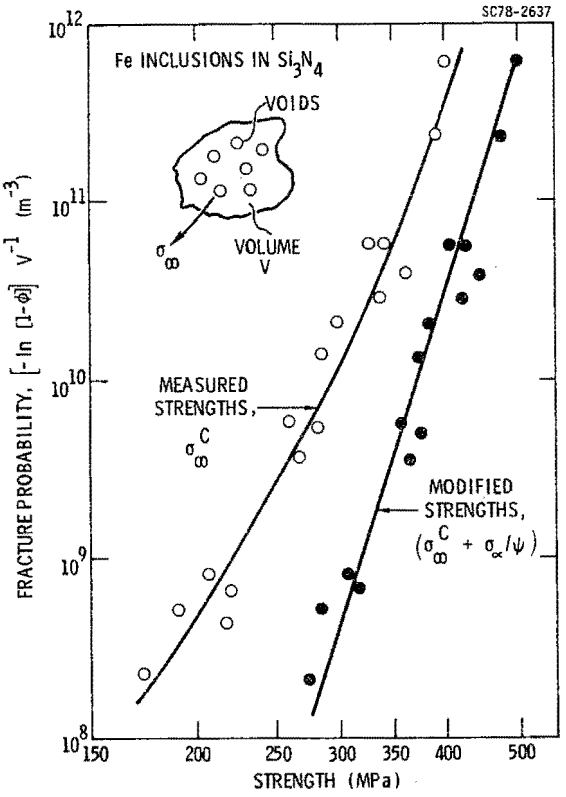

Fig. 6 A plot of the normalized failure probability as a function of the measured strength and the modified strength for iron inclusions in silicon nitride.

Tungsten Carbide Inclusions

The relatively minor effect of the Sl inclusions on the fracture strength of silicon nitride precludes the need for a detailed statistical analysis of strength. The innocuous nature of the tungsten carbide inclusion derives from a combination of relatively high toughness and modulus, as noted above. The analysis of fracture would involve considerations of the distribution of microcracks located with the matrix in the small zone of tension near the poles of the inclusion.[10] The mode of analysis would be essentially similar to that conducted for fracture from voids,[4,5] as modified by the different distribution of matrix stress and the presence of a high toughness inclusion.

IMPLICATIONS AND CONCLUSIONS

Good physical models of the probability of fracture from inclusions can greatly enhance the ability to predict failure from a nondestructive assessment of the inclusion type and size. Models pertinent to specific inclusion types have been presented, and correlations with fracture data have been attempted. The data are not inconsistent with the fracture models. However, to obtain good statistical confidence in the models, additional data are required, for well-controlled inclusion morphologies. Specifically, data sets are required for inclusions of given size, taken at several different size values.

The present results can be used directly in probablistic estimates of reliability, within the strength range that data have been obtained, even though the applicability of the models has not been substantiated with good statistical confidence. The confident substantiation of the present (or alternatives) models of fracture from inclusions would have the advantage of permitting the reliability predictions to be extended beyond the range of the data and, hopefully, to minimize the variance that must be applied to the fracture probability - thereby reducing the rejection probability associated with any given method of nondestructive analysis.

The strong influence of the inclusion type on the fracture strength is re-emphasized. Specifically, tungsten carbide inclusions can be regarded as almost innocuous, while silicon inclusions are extremely deleterious at low temperatures; iron inclusions and voids[5] are of intermediate severity. It is interesting to note that surface cracks in hot-pressed silicon nitride produces about the same strength degradation as silicon inclusions with the equivalent diameter. However, it should be noted that silicon develops appreciable toughness above ~ 1000°C, and melts at 1420°C. Silicon inclusions are thus likely to become less deleterious at elevated temperatures ($\lesssim$ 900°C), tending to approach the behavior of voids of equivalent size.

Finally, the appreciable dependence of the fracture probability on the inclusion type clearly emphasizes the importance of defect type classification for effective nondestructive failure prediction schemes.

APPENDIX I

STRESSES PRODUCED BY THERMAL EXPANSION MISMATCH

The magnitude of the thermal expansion stress depends on the cooling temperature ΔT (Eqn. 1). An exact definition of this temperature differential presents several problems. The stress within the inclusion is purely hydrostatic (i.e., no shear stresses), and stress relaxation can only occur by mass transport processes. By contrast, the stress within the matrix has a zero hydrostatic component, $p(\sigma_{rr} + 2\sigma_{\theta\theta} = 0)$, but a very large shear component, $\sigma_{r\theta}(\equiv 3\beta^*/4)$; relaxation in the matrix can thus also occur by shear processes. The latter is similar to the elastic/plastic deformation of spherical cavity, for which the relative displacement of the cavity surface depends on the yield strength. However, there is no evidence that Si_3N_4 exhibits significant

shear plasticity. It is thus considered that the only appreciable relaxation occurs by mass transport. The chemical potential that acts as the driving force for atom migration is dictated within the inclusion primarily by the hydrostatic pressure

$$\mu_i = -p\Omega \tag{A1}$$

and within the matrix by the strain energy

$$\mu_m = G_m \frac{(\Delta\alpha\Delta T)^2}{[1+2(1-2\nu_i)/(1-\nu_i)(G_m/G_i)]^2}\left[\frac{3}{8(1-\nu_m)} + \frac{9}{16}\right]\left(\frac{R}{r}\right)^6 \tag{A2}$$

where Ω is the atomic volume. The incidence of atom transport will modify the chemical potential and the stress distribution. This will occur primarily by vacancy transport to the interface. However, if the stress within the inclusion is tensile, cavities may nucleate by vacancy condensation. Nucleation will occur when the stress exceeds[16]

$$p^2 \approx \frac{4\alpha_s^3}{kT\ell n(4\pi D_b \delta_b n_o / p\,\Omega^{4/3})} \tag{A3}$$

Once a cavity has nucleated, the stress at the cavity surface and the local chemical potential must be maintained at their equilibrium values

$$p = 2\alpha_s/r \qquad \mu = -\Omega\alpha_s/r \tag{A4}$$

where r is the cavity radius. The chemical potential gradient now favors vacancy diffusion into the cavity, and cavity growth can be anticipated. Hence, if several cavities nucleate, the stresses within the inclusion remain at a moderate level, while mass transport is occurring. It should also be noted that the formation of cavities decreases the modulus G_i of the inclusion. This tends to minimize the stresses that develop on cooling below the temperature at which mass transport eventually ceases.

APPENDIX II

A POSTERIORI MEASUREMENTS OF INCLUSION VOLUME

Most of the naturally occurring inclusions in structural ceramics develop cracks during temperature excursions. Consequently, the inclusions are relatively friable after fracture, and can be readily separated from the matrix by suitable etchants. The remaining void space can then be filled with a low density wax and the density of the ceramic/wax system measured in a density column. This density is directly related to the inclusion volume v, the density of the ceramic host, p_c, and the density of the wax, p_w, as indicated below.

The measured density p' is:

$$p' = (M + m)/(v + v) \tag{A5}$$

where M is the mass of the ceramic, V its volume and m the maxx of the wax contained within the void space. The parameters in Eqn. (A5) that cannot be easily measured are m and V; these can be eliminated from the measurement process by substituting the densities p_w and p_c:

$$v = \left(\frac{M}{p_c}\right)\left[\frac{p_c - p'}{p' - p_w}\right] \tag{A6}$$

The densities p_c and p' can be obtained directly from density column studies, before and after the wax has been inserted into the void space.

ACKNOWLEDGMENT

This research was sponsored by the Center for Advanced NDE, operated by the Science Center, Rockwell International, for the Defense Advanced Research Projects and the Air Force Materials Laboratory under Contract F33615-74-C-5180.

REFERENCES

1. J.R. Richardson and A.G. Evans, to be published.
2. A.G. Evans, Jnl. Mater. Sci. 9 (1976) 1145.
3. F.F. Lange, Fracture Mechanics of Ceramics (Ed. R.C. Bradt, D.P.H. Hasselman, F.F. Lange) Plenum, N.Y. (1978) Vol. 4, p. 799.
4. O. Vardar, I. Finnie, D.R. Biswas and R.M. Fulrath Intl. Jnl. Frac. 13 (1977) 215.
5. A.G. Evans, D.R. Biswas and R.M. Fulrath, Jnl. Amer. Ceram. Soc.,in press.
6. A.G. Evans, G.S. Kino, B.T. Khuri-Yakub and B.R. Tittmann, Materials Evaluation.
7. H.R. Baumgartner, R.H. Brockelman and P.M. Hansen, AMMRC Report, AMMRC TR 78-11 (June 1978).
8. J.B. Wachtman, W. Capps and J. Mandel, Jnl. Materials 7 (1972) 188.

9. J. Selsing, Jnl. Amer. Ceram. Soc. 44 (1961) 419.

10. J.D. Eshelby, Proc. Roy Soc.

11. G.C. Sih, Handbook of Stress Intensity Factors (Lehigh Univ. Press) 1973.

12. S.M. Goldfield and R.E.Quandt, Jnl. Amer. Statistical Assoc., 60, (1965) 539.

13. H. Theil, Jnl. Amer. Statistical Assoc., 60, (1965) 1067.

14. J.R. Matthews, F.A. McClintock and W.J. Shack, Jnl. Amer. Ceram. Soc., 59, (1976) 304.

15. J.J. Petrovic and M.G. Mendiratta, Jnl. Amer. Ceram. Soc. 59 (1976) 163.

16. A.G. Evans, J.R. Rice and J.P. Hirth, to be published.